A major purpose of the Technical Information Center is to provide the broadest dissemination possible of information contained in DOE's Research and Development Reports to business, industry, the academic community, and federal, state and local governments.

Although a small portion of this report is not reproducible, it is being made available to expedite the availability of information on the research discussed herein.

DNF-850840--6

LA-UR--85-1187

DE85 010793

RECEIVED BY OSTI MAY 06 1985

TITLE DEVELOPMENT AND APPLICATION OF THE LOS ALAMOS NUCLEAR MICROPROBE: HARDWARE, SOFTWARE, AND CALIBRATION

AUTHOR(S) T. M. Benjamin, P. S. Z. Rogers, C. J. Duffy, J. F. Conner, C. J. Maggiore, and J. R. Tesmer

SUBMITTED TO 20th Annual Conference of Microbeam Analysis Society, Louisville, KY, August 5-9, 1985.

DISCLAIMER

Los Alamos Los Alamos National Laboratory
Los Alamos, New Mexico 87545

DEVELOPMENT AND APPLICATION OF THE LOS ALAMOS NUCLEAR MICROPROBE: HARDWARE, SOFTWARE, AND CALIBRATION

T. M. Benjamin, F. S. Z. Rogers, C. J. Duffy, J. F. Conner, C. J. Maggiore, and J. W. Tesmer.

There is a great demand for spatially resolved quantitative trace element analyses of geologic samples. This class of samples is characteristically heterogeneous, fine grained, and compositionally complex. The Los Alamos nuclear microprobe has been developed for, and applied to, non-destructive in-situ geochemical analysis, primarily using the proton induced x-ray emission technique (PIXE). Characteristic x-ray spectra are acquired by bombardment with 1 to 200 nA beams of protons from the Los Alamos vertical Van de Graaff accelerator. Beam spot diameters of 10 μm are routine. After spectrum deconvolution, detection limits of approximately 5 ppm are obtained for an integrated charge on the order of 10 μC. Applications, concomitant with development have included analyses of meteorites,[1,2] including one potential sample of Mars,[3] terrestrial oil shales,[4] archaeological artifacts, and ore mineral samples.

Authors Benjamin, Rogers, and Duffy are in the Isotope and Nuclear Chemistry Division, Maggiore is in the Electronics Division, and Tesmer is in the Physics Division. All are at the Los Alamos National Laboratory, Los Alamos, New Mexico. Conner is in the Physics Department, University of California, Davis, California.

[illegible] Auburn [illegible] system,[illegible] [illegible], contains several [illegible] components. [illegible] Van de Graaff accelerator is exceedingly [illegible] [illegible] Faraday cup [illegible] [illegible] to 6.5 MeV. Focused beams on target [illegible] nA. Additionally, a wide variety of positive and negative particle beams can be [illegible] for low Z element analysis by particle induced gamma ray emission (PIGE) and nuclear reaction analysis (NRA),[4] and in Rutherford backscattering (RBS) analysis.[5]

The NbTi superconducting solenoid final lens is critical to the attainment of high current densities and micron scale spots. Unlike quadrupole final lenses, the solenoid can focus ion beams to submicron diameters while retaining a useable 200 pA/μm^2 current density. Magnetic fields up to 80 kilogauss can be produced by the solenoid. Ion optics considerations[5] and the physical dimensions of the solenoid and liquid helium dewar constrain the position of the sample stage and the x-ray detectors, Fig. 2. The solenoid reduces the spot size defined by the selected Pt SEM aperature in the aperture box, Fig. 1, by a factor of 10 when focussed on target. The use of cooled SEM aperatures simplified spot size selection relative to a cooled microjaw slit system.

In addition to a Si(Li) x-ray detector, the sample chamber, Fig. 2, mounts two crystal x-ray spectrometers originally used on a MAC electron microprobe. Mounted horizontally rather than in the normal vertical orientation, due to solenoid defined space constraints and [illegible] to maintain a takeoff angle equal to that of the Si(Li) detector, these spectrometers have proved to be difficult to align. Further effort will solve this problem so that the high degree of x ray wavelength discrimination

characteristic of crystal spectrometers can be used on a PIXE nuclear microprobe system for the first time. Even with poor alignment, we have obtained peak to background ratios that are more than an order of magnitude superior to those obtained with a Si(Li) microprobe. These spectra will radically improve the rare earth element (REE) detection limits compared to Si(Li) spectrum deconvolution results, to the benefit of many meteoritic and terrestrial geochemical problems.

Near term hardware additions will include precise current integration by RBS, secondary electron suppression and on-demand beam deflection to reduce bremsstrahlung, rapid 2D beam scanning, and secondary electron imaging capability.

Software

The software developed at Los Alamos for deconvoluting and quantifying the Si(Li) PIXE data is based on calculations using fundamental parameters. When applied to the data, quantitative results are obtained using only one variable for each element, peak height. The electronic signal amplification gain and zero offset are determined in an energy calibration routine. Weighed least squares fitting of known elemental peaks in spectra from standards and the individual unknowns take into account the discrete x-ray lines in the data peak envelopes (for example, the α_1 and α_2 peaks in a Kα envelope). The x-ray energy dependent gaussian peak half-width function is also calibrated from the same peaks used in the energy calibration. This function, a characteristic of the Si(Li) detector, appears extremely stable and reproducible. The sample spectra are then fit with discrete envelopes composed of the sum of the gaussians for all the lines of each element. Because only one variable per multigaussian envelope, characteristic of each

element, is required [illegible], many overlap problems can be quantitatively resolved while maintaining excellent detection limits. In the case of REE data, several [illegible] of the numerous closely spaced (relative to Si(Li) energy resolution) L-series lines imposed on a non-linear bremsstrahlung background and degrades the detection limits to roughly 100 ppm.

Essential to this method is knowledge of the relative intensities of every x-ray line for each element in that particular matrix so that a single fit parameter per element suffices. Also required are the relative intensities between lines of differing elements so that a known major element can be used as an internal standard for quantification of the abundance of all other elements in the spectrum. These relative intensities are calculated by numerical integration.[7] As the samples are thick targets, the numerical integration includes the effects of decreasing beam energy (and the corresponding x-ray production cross-sections) with depth and x-ray absorption in the sample. As an example, a 2.5 MeV proton beam penetrates 50 μm into quartz but x-rays from elements lighter than Ca, although produced at this depth, do not reach the detector (Na, 17 μm max.; Al, 37 μm max.; and Cl 43 μm max.).

A truly typical spectrum is shown in Fig. 3. The sample, a meteoritic plagioclase that has been impact shocked into a glass was analyzed under the following conditions: 2.5 MeV protons, 9 nA beam current, 10 μm spot, 6.8 μC integrated charge, x-ray filters consisting of 20.335 mg/cm^2 Be and 13.117 mg/cm^2 Al and a numerical integration step size of 1.0 (1.0 = 10 KeV). The elements given in the legend and tabulated in Table 1 were normalized to the electron microprobe value of 6.18 wt% Ca through the relative intensity calculation. The x-ray filters were chosen to suppress the major elements such as Ca in order to minimize detector deadtime. Note that at this plot

[illegible]
Also [illegible] in progress. [illegible] negligible [illegible] to [illegible].

[illegible] that the peak positions and linewidths are determined by least squares calibration and that the α/β ratios are calculated from fundamental parameters, the fit to Si is very good. The sensitivity of the least-squares technique requires consideration of escape and pileup sum peaks. The Fe $K\alpha K\alpha$ sum peak is imperfectly fit although statistically the error is small. The Rb $K\alpha$ and Fe $K\alpha K\beta$ sum peak have a severe overlap. The sum peak proportionality systematics requires the presence of some Rb to adequately model the data.

Development plans include addition of the x-ray fluorescence correction, Lorentzian intrinsic line widths, low energy exponential tails, and bremsstrahlung modeling.

Calibration

Initial calibrations against known materials indicate an accuracy on the order of 10% when a major element is used as an internal standard. Precise current integration by RBS and new trace element standards, both synthetic and natural will permit precise intersample comparison. Calibration and software testing in progress include analyses of a suite of pure metals; simple alloys and minerals used as electron microprobe standards; fused [illegible] of W-1, AGV-1, BCR-1, and BHVO-1 rock standards.

Sensitivity to variations in the beam energy (and, therefore, x-ray production cross-sections), matrix, numerical integration step size, and

beam-to-target and detector-to-target angles (55° and 57°, respectively) is being assessed by calculation.

Examples of the effect of matrix and numerical integration step size are given in Figs. 5 and 6. The two matrices, SiO_2 and Fe_3O_4, encompass the mean atomic number of most geologic materials. The numerical integration step size is in units of 10 KeV. In both Figs 5 and 6 the curves are relative intensity calculations normalized to a 0.2 (that is, 2 KeV) integration step size. In Fig. 5 the x-ray energy dependence (plotted as atomic number for Kα x-rays) vs. the difference (error) in the relative intensities between a step size of 2.0 and a step size of 0.2 is shown. As expected, the larger step size yields poorer results but only for the softer x-rays and at absorption edges. The difference is less than 5% for all elements heavier than Cl (for K-lines, and heavier than Rh for L-lines). Fortunately, the deviations due to step size are linear for reasonable ranges of step size (Fig. 6). This allows, where necessary, extrapolation to zero step size. Again, the softer x-rays are most affected and the matrix effects less significant for the higher atomic number elements. This type of analysis, when extended to other variables in the system will allow the details of the PIXE analysis technique to be tailored to the accuracy required by the particular problem.

Conclusion

The PIXE technique has proven to be a major advancement in in-situ non-destructive spatially resolved trace element analysis. The Los Alamos nuclear microprobe is being developed and calibrated to produce rapid and comprehensive elemental analysis of complex geologic samples with a 5 ppm detection limit.

References

1. T. M. Benjamin et al., "Microprobe analysis of rare earth element fractionation in meteoritic minerals," Nuclear Instruments and Methods, B3, 221, 1984, 677-680.

2. D. S. Woolum et al., "Trace element PIXE studies of Qinzhen (EH3) metal and sulfides," Lunar and Planetary Science XV (abs), 1984, 935-936.

3. J. H. Jones et al., "The youngest meteorites: II. trace element ing in Zagami maskelynite," Lunar and Planetary Science XVI (abs), 1985, (in press).

4. T. M. Benjamin et al., "The application of the Los Alamos nuclear microprobe to the characterization of trace element-mineral associations in geologic materials and solid wastes," Proceedings of the American Nuclear Society, 5th International Conference, Mayaguez, Pureto Rico, 1984, (in press).

5. C. J. Maggiore, "The nuclear microprobe-investigating surfaces with ions," Los Alamos Science, 3, 1982, 27-45.

6. G. Amsel and W. A. Lanford, "Nuclear reaction techniques in materials analysis," Annual Reviews in Nuclear Science, 34, 1984, 435-460.

7. P. S. Z. Rogers et al., "Geochemical applications of nuclear microprobes," Nuclear Instruments and Methods, B3, 231, 1984, 671-676.

TABLE 1.- ... Mo\ PIXE spectrum, ... plagioclase

Element	Concentration (ppm)
P	3700 ± 1400*
Ca	≤6.18 x 10^4
Ti	534 ± 35
Cr	13 ± 7
Mn	131 ± 8
Fe	7550 ± 40
Zn	11 ± 2
Ga	60 ± 4
Ge	2 ± 2
Rb	7 ± 3
Sr	166 ± 12
La	90 ± 50
Ce	30 ± 50

*Errors are 1σ total uncertainty.

FIG. 1.-- Los Alamos nuclear microprobe beam line schematic, side view.

Microprobe Beam Line, Side View

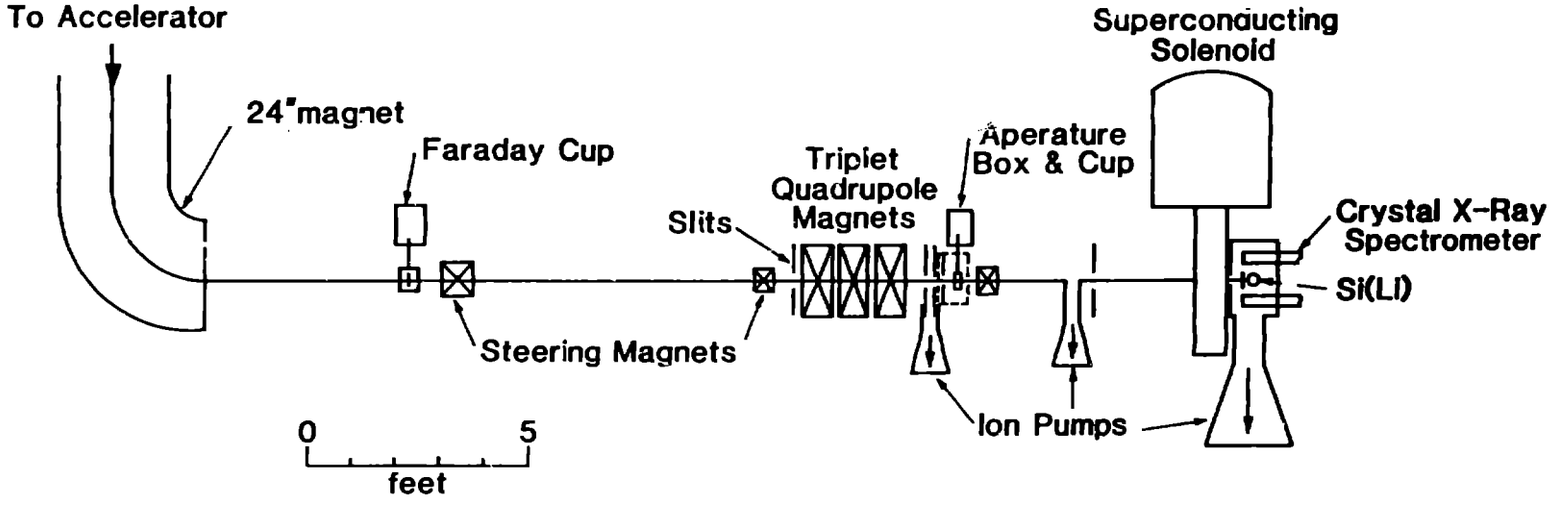

Fig 1

FIG. 2.-- Los Alamos nuclear microprobe sample chamber, top view. Crystal x-ray spectrometers, not shown (see Fig. 1), are mounted above and below Si(Li) detector.

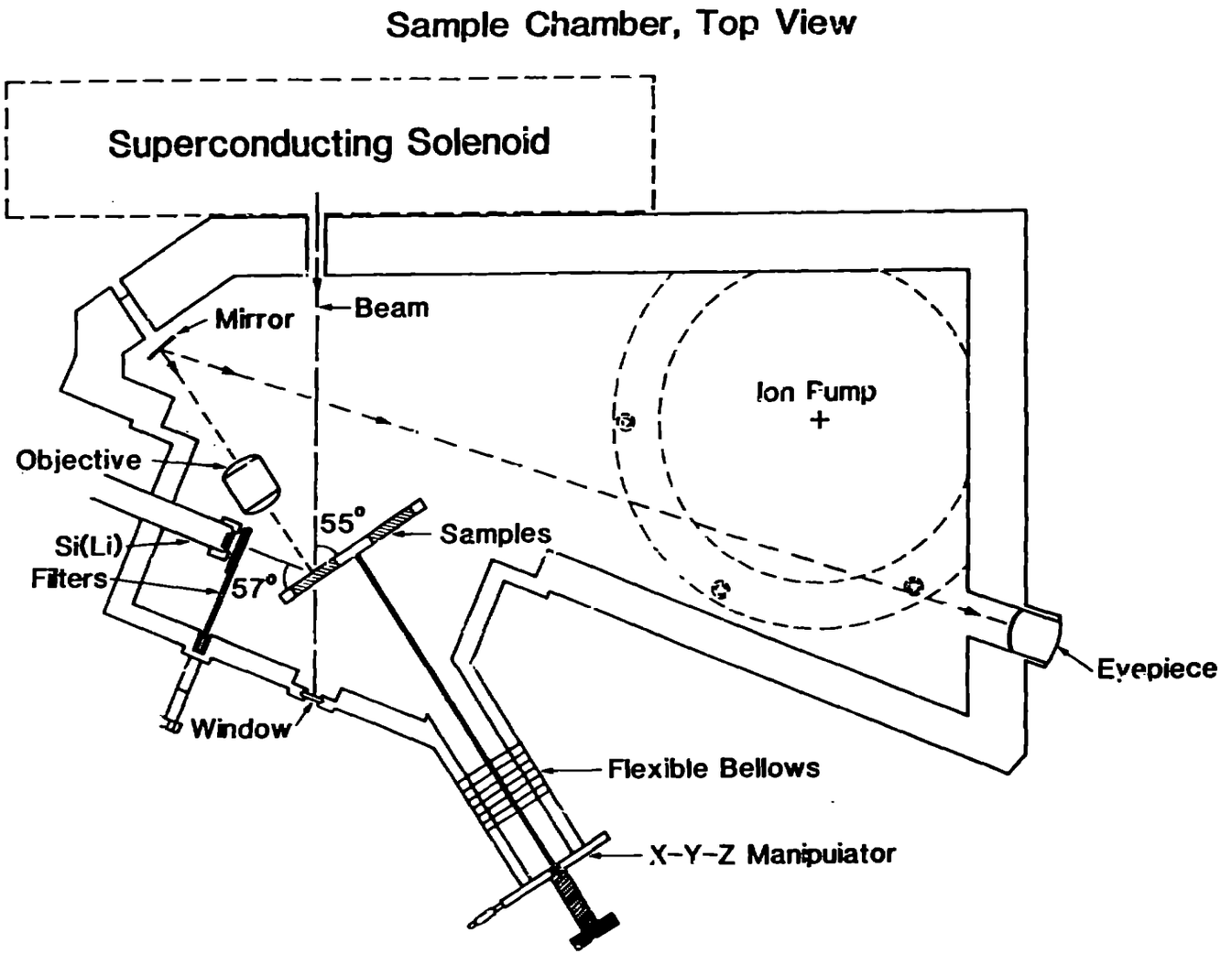
Sample Chamber, Top View
Superconducting Solenoid
Mirror
Beam
Ion Pump
+
Objective
Si(Li)
Filters
55°
57°
Samples
Eyepiece
Window
Flexible Bellows
X-Y-Z Manipulator

Fig 2

FIG. 3.-- 2.5 MeV PIXE spectrum and data deconvolution results for Zagami meteorite shocked plagioclase. Concentrations given in Table 1.

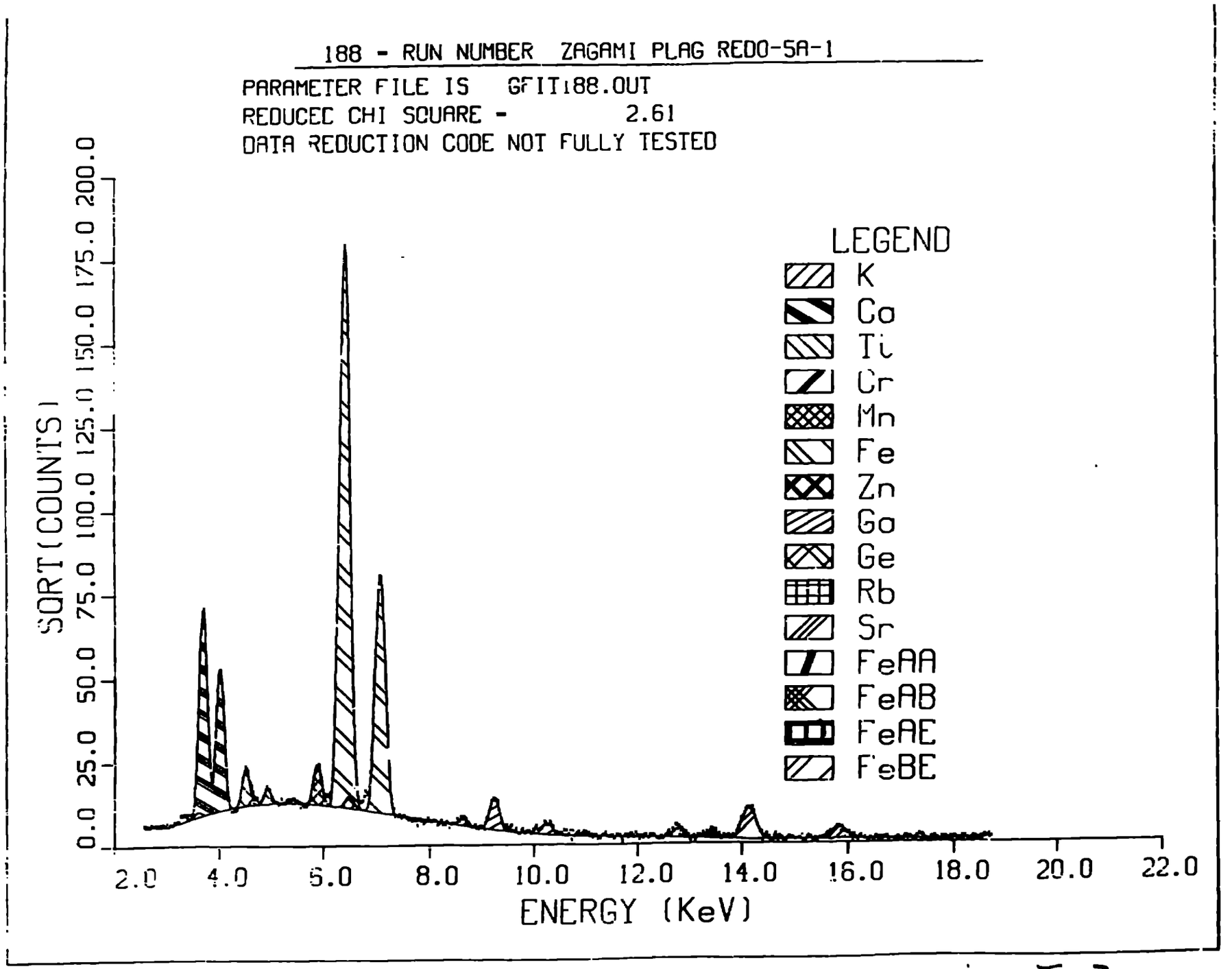
188 - RUN NUMBER ZAGAMI PLAG REDO-5A-1
PARAMETER FILE IS GFIT188.OUT
REDUCED CHI SQUARE - 2.61
DATA REDUCTION CODE NOT FULLY TESTED
LEGEND
K
Ca
Ti
Cr
Mn
Fe
Zn
Ga
Ge
Rb
Sr
FeAA
FeAB
FeAE
FeBE
SQRT(COUNTS)
0.0 25.0 50.0 75.0 100.0 125.0 150.0 175.0 200.0
2.0 4.0 6.0 8.0 10.0 12.0 14.0 16.0 18.0 20.0 22.0
ENERGY (KeV)

Fig 3

FIG. 4.-- Enlarged portion of Fig. 3. showing excellent fit of relative intensity calculation to data.

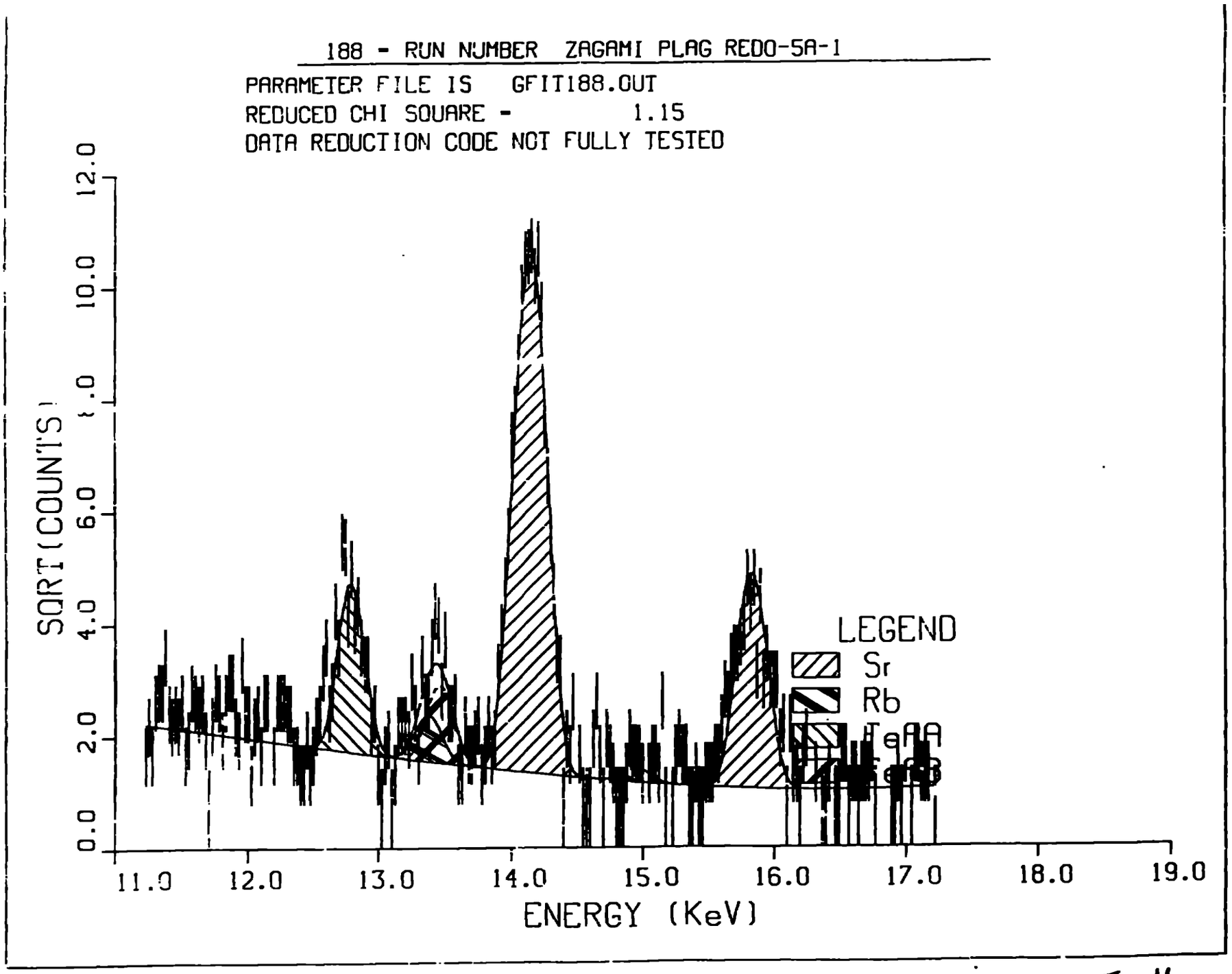
188 - RUN NUMBER ZAGAMI PLAG REDO-5A-1
PARAMETER FILE IS GFIT188.OUT
REDUCED CHI SQUARE - 1.15
DATA REDUCTION CODE NOT FULLY TESTED
SQRT(COUNTS)
0.0
2.0
4.0
6.0
10.0
12.0
11.0
12.0
13.0
14.0
15.0
16.0
17.0
18.0
19.0
ENERGY (KeV)
LEGEND
Sr
Rb

Fig 4

FIG. 5.-- Percentage error as function of x-ray energy (plotted as atomic number for Kα x-rays) and matrix composition for numerical integration step size of 2.0 relative to step size of 0.2.

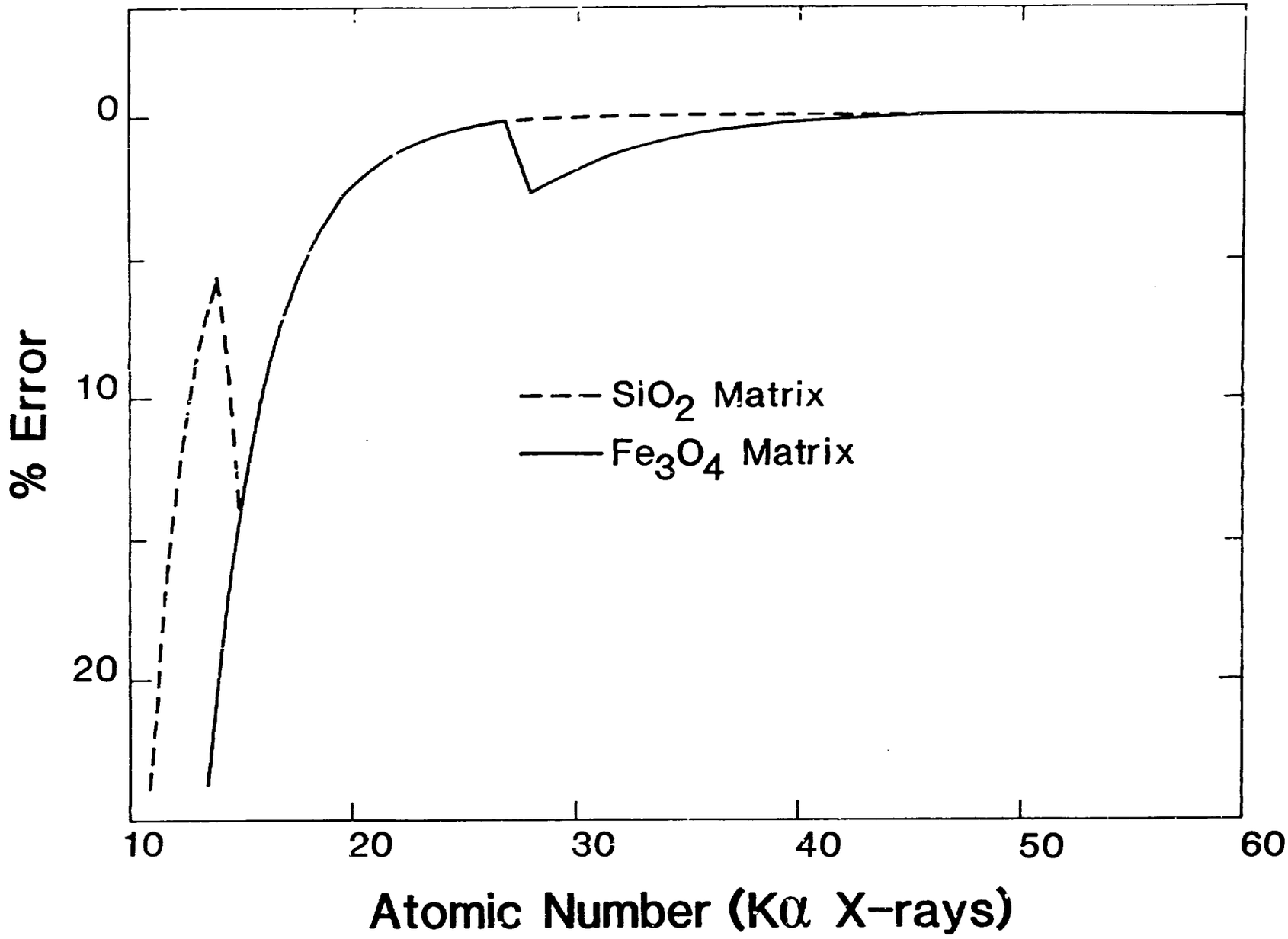
0
10
20
% Error
--- SiO_2 Matrix
—— Fe_3O_4 Matrix
10
20
30
40
50
60
Atomic Number (Kα X-rays)

Fig. 5.

F . 6.-- Deviations in relative intensities as function of step size and matrix composition normalized to step size of 0.2. Results for calcium and iron are nearly coincident and are displaced for clarity.

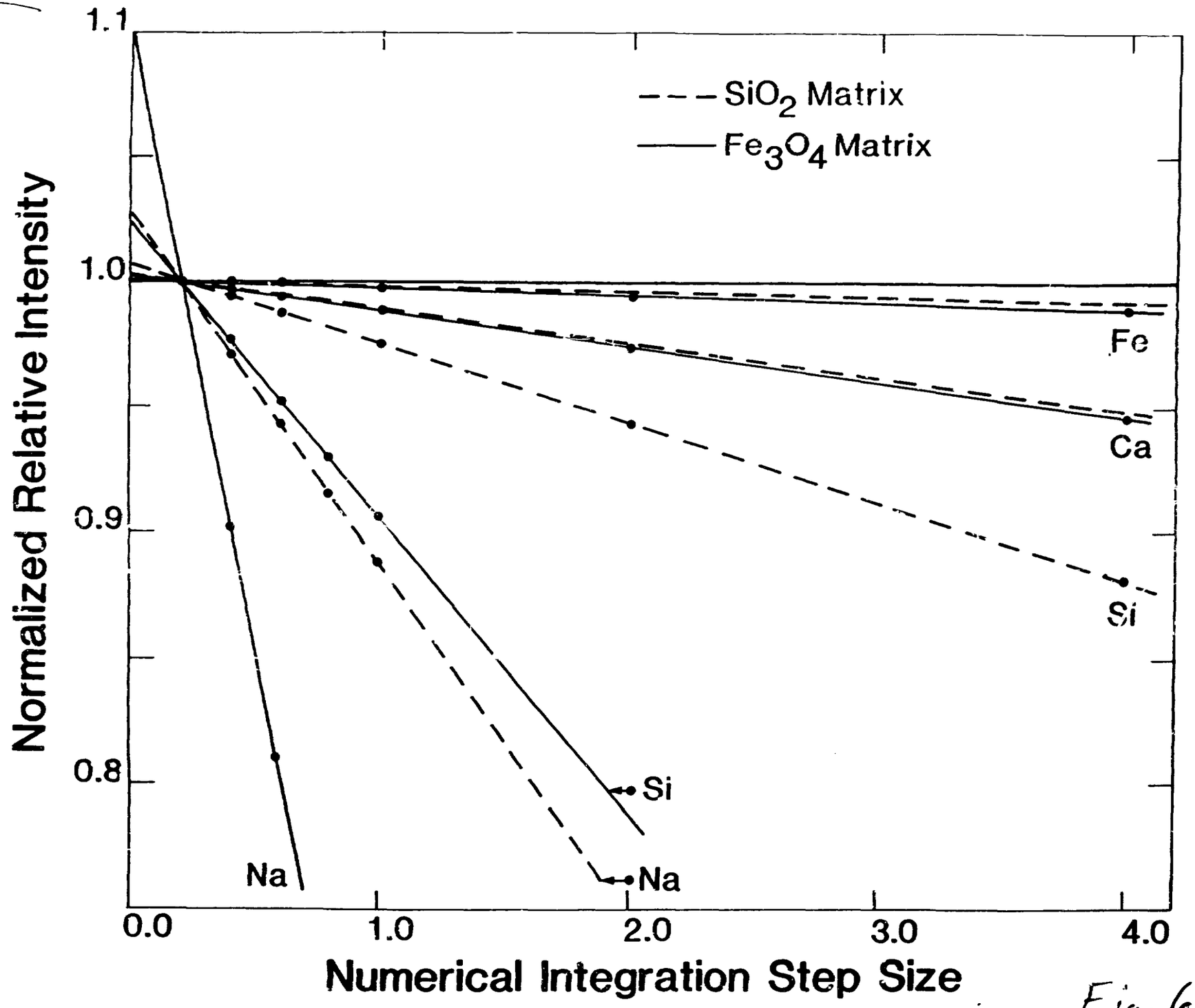
1.1
1.0
0.9
0.8
Normalized Relative Intensity
SiO_2 Matrix
Fe_3O_4 Matrix
Fe
Ca
Si
Si
Na
Na
0.0
1.0
2.0
3.0
4.0
Numerical Integration Step Size

Fig. 6.